Study of interfacial spin transport with an antiferromagnetic Cr_2O_3 interlayer

Ailiang Zou, Ziyang Zhang, Yuekui Xu, Mengyao Du, Xiaolei Wang, Shuo Chang, and Zhiyong Qiu*
Key Laboratory of Materials Modification by Laser, Ion, and Electron Beams (Ministry of Education), School of Materials Science and Engineering, Dalian University of Technology, Dalian 116024, China and Key Laboratory of Energy Materials and Devices (Liaoning Province), School of Materials Science and Engineering, Dalian University of Technology, Dalian 116024, Liaoning, China

(Received 10 October 2021; revised 28 December 2021; accepted 5 January 2022; published 25 January 2022)

Interfacial spin transport has been studied in a YIG/Cr_2O_3/Pt trilayer device via the spin-pumping technique. It is found that the linewidths and the magnitudes of the spin-pumping voltage signals suddenly decrease at just below the Néel temperature of the Cr_2O_3 interlayer. A detailed analysis shows that the inner decay in the Cr_2O_3 interlayer dominates the interfacial spin transport in a wide temperature range, while the interfacial suppression of pumped spin currents occurs at a temperature slightly lower than the Néel temperature, both of which contribute to the sudden changes of spin-pumping voltage signals around the Néel temperature. This work carries forward the understanding of the spin transport in an antiferromagnetic system, which would serve to inspire, as well as facilitate, further breakthroughs of the limits of spin-based devices.

DOI: 10.1103/PhysRevB.105.014427

I. INTRODUCTION

Electronic spins have been considered to serve as the carriers of information and energy in the next-generation information processing devices [1]. Therefore, the study of the spin transport in various condensed matter systems is a fundamental requirement for developing spin-based devices. Here, antiferromagnetic materials as new types spin functional materials have achieved widespread attention due to the great potential for applications, such as memory and spin-based logic devices [2–6]. Especially, antiferromagnetic insulators, in which spins are carried by spin waves unaccompanied with charge currents [7–11], have been looked at as a promising choice for functional cores in high-performance and energy-efficient spin-based devices [5,12]. Novel spin-related effects have been discovered frequently in antiferromagnetic insulators [13–16], in which the spin colossal magnetoresistance as a typical effect has been reported in an antiferromagnetic Cr_2O_3 interlayer [13]. However, the details of spin transport in such nanometer-scale Cr_2O_3 interlayers are still unknown.

For the spin colossal magnetoresistance, Cr_2O_3, a uniaxial antiferromagnet, plays a functional key role. Cr_2O_3 becomes a spin conductor at high temperature [Fig. 1(a)] and suddenly changes into a spin insulator in a narrow temperature window at just below the Néel temperature. Furthermore, this spin conductor-insulator transition can be modulated by an external magnetic field, which results in a more than 500% change of spin transmission. The spin colossal magnetoresistance has been attributed to the anisotropic spin transmissivity of antiferromagnetic Cr_2O_3 in combination with the device geometry. In other words, the spin transport is blocked by a Cr_2O_3 interlayer when the direction of the spin polarization at the interface is perpendicular to the Néel vector of Cr_2O_3 [13]. However, it is still unknown how the spin currents are blocked by a nanometer-scale Cr_2O_3 interlayer.

As shown in Figs. 1(b) and 1(c), there are two possibilities that result in this spin-blocking effect with an antiferromagnetic Cr_2O_3 interlayer at a temperature below the Néel temperature. One is that the spin currents can be injected into the Cr_2O_3 layer but dissipated wholly due to the abrupt decrease of the spin diffusion length [Fig. 1(b)]. Another possibility is that the spin currents cannot be injected into the Cr_2O_3 layer, which are just blocked at the yttrium iron garnet (YIG)/Cr_2O_3 interface [Fig. 1(c)]. It is worth further discussion to clarify this confusion in such a system, which will be helpful for understanding the spin transport phenomena and inspiring new applications.

II. EXPERIMENTAL

In this paper, a YIG/Cr_2O_3/Pt trilayer device was prepared with the same structure as in our previous work [13]. By using this device, spin pumping has been well studied, and the spin conductor-insulator transition was well reproduced. Furthermore, by analyzing the linewidths and magnitudes of the spin-pumping voltage signals in the temperature domain, the transport processes in the Cr_2O_3 interlayer were systematically discussed. The result suggests that both cases in Figs. 1(b) and 1(c) contribute to the spin conductor-insulator transition that occurred at around the Néel temperature.

A trilayer device is fabricated to study the spin transport via the spin-pumping effect [17], in which an antiferromagnetic Cr_2O_3 layer is sandwiched between a magnetic insulator YIG layer and a heavy metal Pt layer [Fig. 2(a)]. The single-crystal YIG layer was grown on a (111) $Gd_3Ga_5O_{12}$ wafer by a liquid phase epitaxy method. The thickness of the YIG layer is about 3 μm, which gave us a high quality crystal [18].

*Corresponding author: qiuzy@dlut.edu.cn

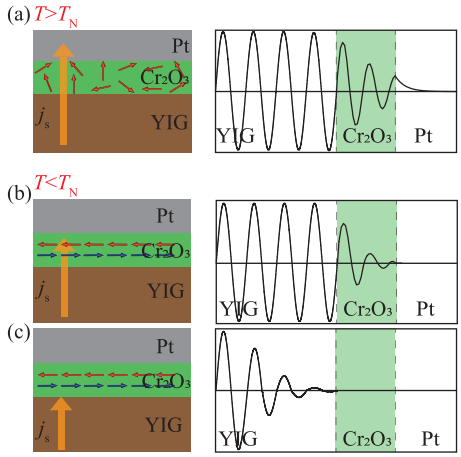

FIG. 1. The concepts of spin transport in a YIG/Cr_2O_3/Pt trilayer device. (a) Spins can transport through the paramagnetic Cr_2O_3 interlayer above the Néel temperature T_N. Here, spins are carried by the thermal magnons excited in the Cr_2O_3 interlayer. When the temperature is lower than the Néel temperature T_N, the spin transport is blocked by the antiferromagnetic Cr_2O_3 interlayer due to the dissipation inside of the Cr_2O_3 interlayer (b), and/or the suppression at the YIG/Cr_2O_3 interface (b).

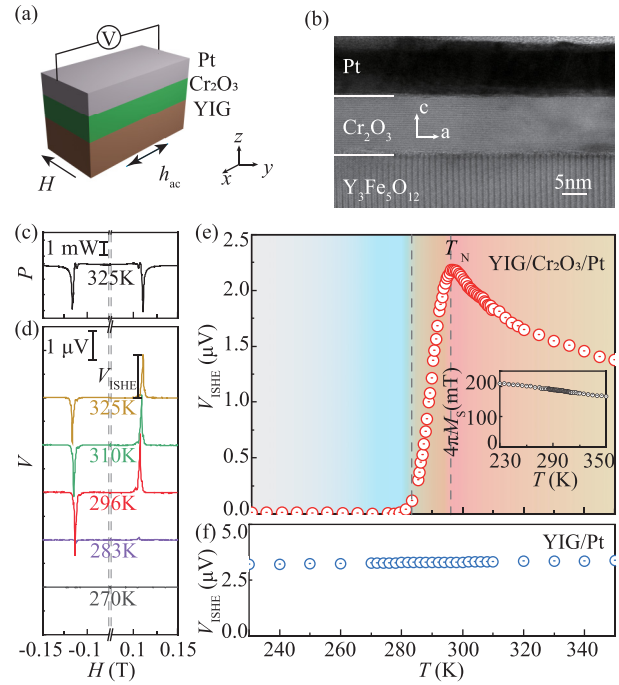

FIG. 2. The experimental setup and the results of the spin-pumping measurement. (a) The schematic of the sample and experimental setup of the spin-pumping effect. (b) A cross-sectional transmission electron microscopy (TEM) image of the YIG/Cr_2O_3/Pt trilayer device. (c) A microwave absorption spectrum at 325 K for the YIG/Cr_2O_3/Pt trilayer device. (d) The external magnetic field H dependences of the voltage signal V at various temperatures for the YIG/Cr_2O_3/Pt trilayer device. (e) The temperature dependence of the spin-pumping voltage V_{ISHE} for the YIG/Cr_2O_3/Pt trilayer device. The inset shows the temperature dependence of $4\pi M_s$ for the YIG layer. (f) The temperature dependence of the spin-pumping voltage V_{ISHE} for the YIG/Pt bilayer device.

The sample was cut into a size of 1.5 mm × 3 mm. Then a 12-nm-thick Cr_2O_3 layer was grown on top of the YIG film at 673 K, followed by a subsequent annealing process for 30 min at 1073 K in a pulsed laser deposition system. Finally, a 10-nm-thick Pt layer was coated on the Cr_2O_3 layer by a radio-frequency magnetron sputtering method.

Figure 2(b) shows the cross-section image of our YIG/Cr_2O_3/Pt trilayer device taken by transmission electron microscopy. It is clear that the YIG layer is of a single-crystal structure, whose [111] direction is along the out-of-plane direction of the sample. The Cr_2O_3 layer exhibits a single-crystal-like structure, whose easy axis (the c axis) is also along the out-of-plane direction. The interfaces of the device are sharp and uniform. The thicknesses of the Cr_2O_3 and Pt layers are 12 and 10 nm, respectively.

Spin transport was studied via the spin-pumping technique [Fig. 2(a)] [7,13,19,20]. In our trilayer device, the YIG layer acts as the spin generator. By applying a microwave and an external magnetic field, ferromagnetic resonance (FMR) is excited in the YIG layer. In this work, the frequency of the microwave is fixed at 5 GHz. Then, spins accumulate at the YIG/Cr_2O_3 interface, which may inject spin currents into the Cr_2O_3 interlayer. If the spin currents can transport through the Cr_2O_3 interlayer, then they can be converted into measurable spin-pumping voltage signals in the Pt layer via the inverse spin Hall effect (ISHE) [21]. Here, the Pt layer acts as the spin detector. The spin-pumping voltage signals can be used to analyze the spin transport phenomena in such a system with a Cr_2O_3 interlayer.

III. RESULTS AND DISCUSSION

Figure 2(c) shows a typical microwave absorption spectrum measured at $T = 325$ K. It is clear that two absorption peaks appeared symmetrically at $H_{FMR} \approx \pm 0.111$ T. Here, H_{FMR} refers to the magnetic field of the FMR condition for the YIG layer. As shown in Fig. 2(d), the voltage peaks can be found at the same magnetic field H_{FMR} with the same temperature. The signs of the voltage peaks were reversed by reversing the external magnetic field, which agrees well with the prediction of the spin-pumping effect [17]. Those voltage peaks can be attributed to the pumped spin currents from the YIG layer through the Cr_2O_3 interlayer, which are detected via ISHE in the Pt layer. Here, we defined the heights of those voltage peaks as the spin-pumping voltage V_{ISHE} [Fig. 2(d)].

The magnetic field H dependences of the electric voltage V at various temperatures are shown in Fig. 2(d). With decreasing temperature, the positions of the voltage peaks shift toward the low magnetic field. This can be attributed to the changing H_{FMR} corresponding to the increasing saturation magnetization $4\pi M_s$ of the YIG layer [22]. By using the Kittel's formula [23], $4\pi M_s$ at various temperatures are estimated and shown in the inset of Fig. 2(e). The $4\pi M_s$ of the YIG layer changes smoothly and the changing ratio is only about -0.37 mT/K in the temperature range from 230 to 350 K. At all temperatures, the signs of those voltage peaks are reversed when the applied magnetic field is reversed, further confirming that

the voltage peaks are related to the spin-pumping effect. The magnitude of the spin-pumping voltage V_{ISHE} decreases suddenly when the temperature T is lower than 296 K, and even merges into the noise level at the temperature around 280 K.

The spin-pumping voltages V_{ISHE} at various temperatures are plotted on the temperature domain [Fig. 2(e)]. The spin-pumping voltage V_{ISHE} gradually increases toward a maximum at around 296 K with decreasing temperature from 350 K, then decreases suddenly to the noise level in a narrow temperature window. Here, 296 K is the Néel temperature of the Cr_2O_3 interlayer [24,25]. If we consider the YIG layer as a constant spin source, the magnitude of V_{ISHE} directly relates to the spin transmission of the Cr_2O_3 interlayer in our setup. Therefore, the result suggests that Cr_2O_3 is a spin conductor at the high-temperature paramagnetic phase and becomes a spin insulator at the low-temperature antiferromagnetic phase. In contrast, the device without the Cr_2O_3 interlayer does not show such a sudden suppression of the spin-pumping voltages in the same temperature range [Fig. 2(f)], which agrees well with the published results [26–28].

In the model of the spin-pumping effect [29], the "pumping" of spins slows down the precession of local spins corresponding to an enhancement of the Gilbert damping constant α. Here, α is usually estimated by the linewidth Γ of the microwave absorption spectrum as $\alpha = \gamma/2\pi f$, where γ and f are the gyromagnetic ratio of the magnetic layer and the frequency of the applying microwave. Because the YIG layer in our device is thicker than 3 μm and the width of the coplanar waveguide is about 0.5 mm, the microwave absorption should cross the whole YIG layer, but only a thin layer close to the interface contributes to the spin pumping in which the Gilbert damping constant will be enhanced [30]. Therefore, the measurable enhanced Gilbert damping constant $\Delta\alpha$ from a microwave absorption spectrum will be small, which is even impossible to quantify due to the average effect for the thick magnetic layer [31]. Instead, the spin-pumping voltage signals reflect the resonance features of the pumped spins only, which are more suitable for the spin-current estimation of a thick magnetic layer. In this work, the Gilbert damping constant α_v was estimated from the spin-pumping voltage to analyze the details of the spin transport phenomenon in the trilayer device with the Cr_2O_3 interlayer.

From the spin-pumping model [17,29], the pumped spin currents can be described as

$$j_s^0 = \frac{g_r^{\uparrow\downarrow}\gamma^2 h^2 \hbar[4\pi M_s\gamma + \sqrt{(4\pi M_s)^2\gamma^2 + 4f^2}]}{8\pi\alpha^2[(4\pi M_s)^2\gamma^2 + 4f^2]}, \quad (1)$$

$$g_r^{\uparrow\downarrow} = \frac{4\pi M_s d_{\mathrm{eff}}}{g\mu_B}(\alpha_v - \alpha_0). \quad (2)$$

Here, g, μ_B, $\hbar$, and $g_r^{\uparrow\downarrow}$ are the Landé g factor, the Bohr magneton, the reduced Planck constant, and the real part of the spin mixing conductance. f is the frequency of the applying microwave which is fixed at 5 GHz. h is the amplitude of the microwave magnetic field, and h^2 is proportional to the absorption power of the microwave which was carefully maintained at various temperatures in this work. The influence of $4\pi M_s$ is neglected in the following discussion as it is calculated that $4\pi M_s$ changes j_s^0 less than 2.6% in the temperature range from 230 to 350 K. Therefore, j_s^0 can be simplified to $j_s^0 \propto g_r^{\uparrow\downarrow} \propto d_{\mathrm{eff}}$ (α_v-α_0) by removing all the physical constants and the fixed experimental parameters. Here, d_{eff} refers to the effective thickness in the YIG layer that contributes to the spin-pumping effect, which can also be simplified as a constant for the same magnetic layer [32]. α_0 is the intrinsic Gilbert damping constant of the YIG layer without a conjunct layer.

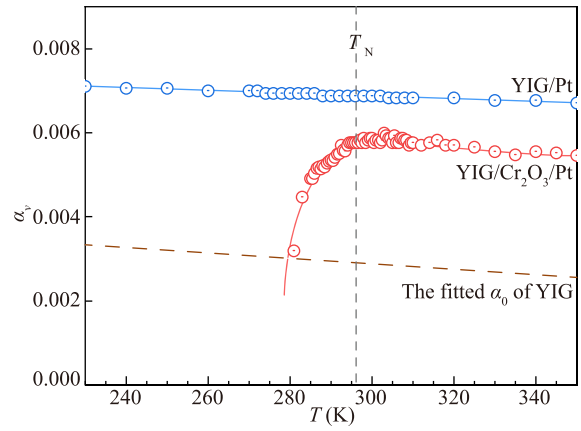

FIG. 3. The temperature dependences of the Gilbert damping constant α_v for the YIG/Cr_2O_3/Pt trilayer and the YIG/Pt bilayer devices, which are estimated from the spin-pumping voltage signals. The dashed line is the fitted intrinsic α_0 of the YIG layer.

In Fig. 3, the temperature dependences of α_v for the YIG/Cr_2O_3/Pt trilayer and the YIG/Pt bilayer devices are shown. For the YIG/Pt bilayer device, α_v increases gradually and monotonously with decreasing temperature, which well agrees with the trend of V_{ISHE} at the same temperature range. This implies that the Pt layer can act as a stable spin detector and the interfacial efficiency of spin transport is almost consistent at different temperatures. On the other hand, for the YIG/Cr_2O_3/Pt trilayer device, the α_v smoothly increases first and then decreases suddenly at $T < 296$ K. When the temperature is lower than 280 K, the spin-pumping voltage signal V_{ISHE} is too small to estimate. These results suggest that the pumped spin currents j_s^0 in the YIG/Cr_2O_3/Pt trilayer device are suddenly suppressed at just below the Néel temperature, which could be a reason for the spin conductor-insulator transition.

The magnitude of V_{ISHE} is proportional to the intensity of the spin currents transported through the Cr_2O_3 interlayer. Considering the inner decay of spin currents in the Cr_2O_3 interlayer, an additional factor D is added into the foundational model [17], then the spin-pumping voltage signal V_{ISHE} can be described as

$$V_{\mathrm{ISHE}} = DR\theta_{\mathrm{SHE}}\lambda \tanh(d_{\mathrm{Pt}}/2\lambda)\left(\frac{2e}{\hbar}\right)j_s^0. \quad (3)$$

Here, R, θ_{SHE}, λ, and d_{Pt} denote the internal resistance, the spin Hall angle, the spin diffusion length, and the thickness of the Pt layer, respectively. D is the inner decay factor of spins in the Cr_2O_3 interlayer, which should be smaller than 1 as spins should always dissipate during its transport. For a bilayer device without a Cr_2O_3 interlayer, we simply take $D = 1$. Therefore, if we compare the YIG/Cr_2O_3/Pt trilayer

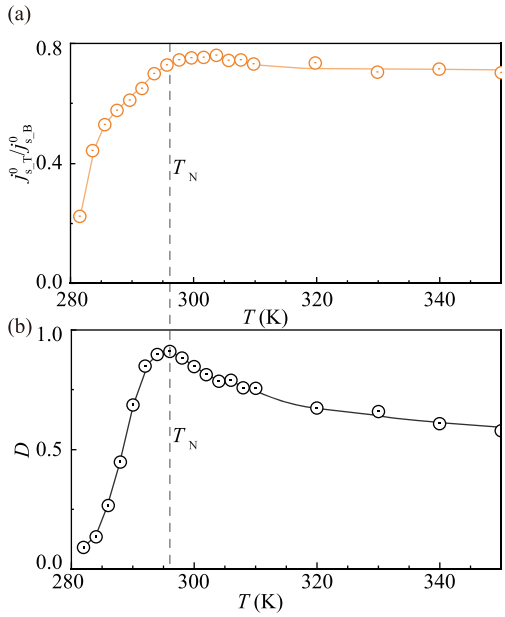

FIG. 4. (a) The temperature dependence of $j^0_{s\_T}/j^0_{s\_B}$. (b) The temperature dependence of the inner decay factor D.

and the YIG/Pt bilayer devices directly, V_{ISHE} and the Gilbert damping constant can be related as

$$\frac{V_{ISHE\_T}}{V_{ISHE\_B}} = \frac{D j^0_{s\_T}}{j^0_{s\_B}} = \frac{D(\alpha_{v\_T} - \alpha_0)}{\alpha_{v\_B} - \alpha_0}. \quad (4)$$

Here, subscripts T and B refer to YIG/Cr_2O_3/Pt trilayer and YIG/Pt bilayer devices, respectively. By Eq. (4), $j^0_{s\_T}/j^0_{s\_B}$ and D can be estimated from V_{ISHE} and α_v for the YIG/Cr_2O_3/Pt and the Cr_2O_3/Pt bilayer devices, whose temperatures are shown in Fig. 4. Here, α_0 was taken from our experience, which is shown as the dashed line in Fig. 3.

At temperatures higher than 296 K, $j^0_{s\_T}/j^0_{s\_B}$ is almost constant. It suggests that the pumped spin currents j^0_s operate with a similar temperature dependence in the two devices. The difference between $j^0_{s\_T}$ and $j^0_{s\_B}$ can be attributed to the different mixing conductance due to the different interfacial conditions. In contrast, the inner decay factor D of the Cr_2O_3 interlayer increases significantly with decreasing temperature, which dominates the spin transport efficiency in the trilayer device at the high-temperature paramagnetic phase. This further evidences that the main carriers of spins in such an antiferromagnetic system as Cr_2O_3 are thermal magnons, which continuously evolve into thermal spin fluctuations above the Néel temperature to reduce the transport efficiency of spin at high temperatures. In other words, spin currents in the Cr_2O_3 layer will decay significantly with increasing temperature in the paramagnetic phase due to the evolution of thermal magnons [7,33].

When the temperature is lower than 296 K, the inner decay factor D decreases rapidly within a very narrow temperature window. The sudden suppression can be attributed to the shutdown of the spin transport channel due to the orthogonality of the Néel vector and the spin polarization direction, which has been predicted in our previous work [13]. The anisotropic dispersion of magnons in such a uniaxial antiferromagnet should be the main reason for this sudden change of the inner decay factor D. Surprisingly, at a slightly lower temperature, $j^0_{s\_T}/j^0_{s\_B}$ also decreases with decreasing temperature, which implies that the pumped spin currents $j^0_{s\_T}$ are also suppressed at the interface around the Néel temperature. This suppression can be attributed to the change of spin mixing conductances of the YIG/Cr_2O_3 interface [17,29]. The change of the interfacial interaction between the magnetic moments of YIG and Cr_2O_3 should be the main reason that the pumped spin currents are quite different at both sides of the Néel temperature. It is also this interaction between YIG and Cr_2O_3 magnetic moments that makes antiferromagnetic order at the interface build up at a slightly lower temperature than the bulk part of the Cr_2O_3 layer. Thus, the interfacial suppression of pumped spin currents occurs at a temperature slightly lower than the Néel temperature.

IV. SUMMARY

In the framework of the spin-pumping technique, the spin transport phenomena with an additional Cr_2O_3 interlayer were studied systematically by a comparison with a YIG/Pt bilayer device. It is found that the inner decay of spins in the Cr_2O_3 interlayer is the dominant factor for the spin transport in a wide temperature range. The interfacial suppression of pumped spin currents also contributes to the spin conductor-insulator transition at temperatures lower than the Néel temperature. Our results promote the understanding of spin transport at an interface with an antiferromagnetic interlayer, which will broaden our horizon for applying antiferromagnetic systems in spin-based devices.

ACKNOWLEDGMENT

This work was supported by the National Natural Science Foundation of China (Grants No. 11874098 and No. 52171173), and the Fundamental Research Funds for the Central Universities (DUT20LAB111).

[1] S. A. Wolf, D. D. Awschalom, R. A. Buhrman, J. M. Daughton, S. von Molnár, M. L. Roukes, A. Y. Chtchelkanova, and D. M. Treger, Spintronics: A spin-based electronics vision for the future, Science **294**, 1488 (2001).

[2] H. Yan, Z. Feng, P. Qin, X. Zhou, H. Guo, X. Wang, H. Chen, X. Zhang, H. Wu, C. Jiang, and Z. Liu, Electric-field-controlled antiferromagnetic spintronic devices, Adv. Mater. **32**, 1905603 (2020).

[3] K. Olejník, V. Schuler, X. Marti, V. Novák, Z. Kašpar, P. Wadley, R. P. Campion, K. W. Edmonds, B. L. Gallagher, J. Garces, M. Baumgartner *et al.*, Antiferromagnetic CuMnAs multi-level memory cell with microelectronic compatibility, Nat. Commun. **8**, 15434 (2017).

[4] T. Nozaki and M. Sahashi, Magnetoelectric manipulation and enhanced operating temperature in antiferromagnetic Cr_2O_3 thin film, Jpn. J. Appl. Phys. **57**, 0902A2 (2018).

[5] W. Yu, J. Lan, and J. Xiao, Magnetic Logic Gate Based on Polarized Spin Waves, Phys. Rev. Applied **13**, 024055 (2020).

[6] X. Chen, A. Hochstrat, P. Borisov, and W. Kleemann, Magnetoelectric exchange bias systems in spintronics, Appl. Phys. Lett. **89**, 202508 (2006).

[7] Z. Qiu, J. Li, D. Hou, E. Arenholz, A. T. N'Diaye, A. Tan, K. Uchida, K. Sato, S. Okamoto, Y. Tserkovnyak *et al.*, Spin-current probe for phase transition in an insulator, Nat. Commun. **7**, 12670 (2016).

[8] S. Takei, B. I. Halperin, A. Yacoby, and Y. Tserkovnyak, Superfluid spin transport through antiferromagnetic insulators, Phys. Rev. B **90**, 094408 (2014).

[9] K. Uchida, S. Takahashi, K. Harii, J. Ieda, W. Koshibae, K. Ando, S. Maekawa, and E. Saitoh, Observation of the spin Seebeck effect, Nature (London) **455**, 778 (2008).

[10] Y. Kajiwara, K. Harii, S. Takahashi, J. Ohe, K. Uchida, M. Mizuguchi, H. Umezawa, H. Kawai, K. Ando, K. Takanashi, S. Maekawa *et al.*, Transmission of electrical signals by spin-wave interconversion in a magnetic insulator, Nature (London) **464**, 262 (2010).

[11] L. J. Cornelissen, J. Liu, R. A. Duine, J. Ben Youssef, and B. J. van Wees, Long-distance transport of magnon spin information in a magnetic insulator at room temperature, Nat. Phys. **11**, 1022 (2015).

[12] T. H. Kim, S. H. Han, and B. K. Cho, Chiral-induced switching of antiferromagnet spins in a confined nanowire, Commun. Phys. **2**, 41 (2019).

[13] Z. Qiu, D. Hou, J. Barker, K. Yamamoto, O. Gomonay, and E. Saitoh, Spin colossal magnetoresistance in an antiferromagnetic insulator, Nat. Mater. **17**, 577 (2018)

[14] P. Muduli, R. Schlitz, T. Kosub, R. Hübner, A. Erbe, D. Makarov, and S. T. B. Goennenwein, Local and nonlocal spin Seebeck effect in lateral Pt-Cr_2O_3-Pt devices at low temperatures, APL Mater. **9**, 021122 (2021).

[15] M. W. Daniels, W. Yu, R. Cheng, J. Xiao, and D. Xiao, Topological spin Hall effects and tunable skyrmion Hall effects in uniaxial antiferromagnetic insulators, Phys. Rev. B **99**, 224433 (2019).

[16] A. Qaiumzadeh, H. Skarsvåg, C. Holmqvist, and A. Brataas, Spin Superfluidity in Biaxial Antiferromagnetic Insulators, Phys. Rev. Lett. **118**, 137201 (2017).

[17] K. Ando, S. Takahashi, J. Ieda, Y. Kajiwara, H. Nakayama, T. Yoshino, K. Harii, Y. Fujikawa, M. Matsuo, S. Maekawa, and E. Saitoh, Inverse spin-Hall effect induced by spin pumping in metallic system, J. Appl. Phys. **109**, 103913 (2011).

[18] J. M. Robertson, Liquid phase epitaxy of garnets, J. Cryst. Growth **45**, 233 (1978).

[19] L. Baldrati, C. Schneider, T. Niizeki, R. Ramos, J. Cramer, A. Ross, E. Saitoh, and M. Kläui, Spin transport in multilayer systems with fully epitaxial NiO thin films, Phys. Rev. B **98**, 014409 (2018).

[20] Z. Qiu, T. An, K. Uchida, D. Hou, Y. Shiomi, Y. Fujikawa, and E. Saitoh, Experimental investigation of spin Hall effect in indium tin oxide thin film, Appl. Phys. Lett. **103**, 182404 (2013).

[21] E. Saitoh, M. Ueda, H. Miyajima, and G. Tatara, Conversion of spin current into charge current at room temperature: Inverse spin-Hall effect, Appl. Phys. Lett. **88**, 182509 (2006).

[22] I. Laulicht, J. T. Suss, and J. Barak, The temperature dependence of the ferromagnetic and paramagnetic resonance spectra in thin yttrium-iron-garnet films, J. Appl. Phys. **70**, 2251 (1991).

[23] C. Kittel, On the theory of ferromagnetic resonance absorption, Phys. Rev. **73**, 155 (1948).

[24] D. Tobia, E. Winkler, R. D. Zysler, M. Granada, and H. E. Troiani, Size dependence of the magnetic properties of antiferromagnetic Cr_2O_3 nanoparticles, Phys. Rev. B **78**, 104412 (2008).

[25] S. P. Pati, M. Al-Mahdawi, S. Ye, Y. Shiokawa, T. Nozaki, and M. Sahashi, Finite-size scaling effect on Néel temperature of antiferromagnetic Cr_2O_3 (0001) films in exchange-coupled heterostructures, Phys. Rev. B **94**, 224417 (2016).

[26] R. Sha, Q. Liu, M. Wang, M. Liu, Y. Peng, Z. Zhang, A. Zou, Y. Xu, X. Jiang, and Z. Qiu, Spin transport in different oxide phases of copper, Phys. Rev. B **103**, 024432 (2021).

[27] Y. M. Lu, Y. Choi, C. M. Ortega, X. M. Cheng, J. W. Cai, S. Y. Huang, L. Sun, and C. L. Chien, Pt Magnetic Polarization on $Y_3Fe_5O_{12}$ and Magnetotransport Characteristics, Phys. Rev. Lett. **110**, 147207 (2013).

[28] Y. S. Chen, J. G. Lin, S. Y. Huang, and C. L. Chien, Incoherent spin pumping from YIG single crystals, Phys. Rev. B **99**, 220402 (2019).

[29] Y. Tserkovnyak, A. Brataas, and G. E. W. Bauer, Enhanced Gilbert Damping in Thin Ferromagnetic Films, Phys. Rev. Lett. **88**, 117601 (2002).

[30] M. B. Jungfleisch, A. V. Chumak, A. Kehlberger, V. Lauer, D. H. Kim, M. C. Onbasli, C. A. Ross, M. Kläui, and B. Hillebrands, Thickness and power dependence of the spin-pumping effect in $Y_3Fe_5O_{12}$/Pt heterostructures measured by the inverse spin Hall effect, Phys. Rev. B **91**, 134407 (2015).

[31] M. Haertinger, C. H. Back, J. Lotze, M. Weiler, S. Geprägs, H. Huebl, S. T. B. Goennenwein, and G. Woltersdorf, Spin pumping in YIG/Pt bilayers as a function of layer thickness, Phys. Rev. B **92**, 054437 (2015).

[32] T. Kikkawa, K. Uchida, S. Daimon, Z. Qiu, Y. Shiomi, and E. Saitoh, Critical suppression of spin Seebeck effect by magnetic fields, Phys. Rev. B **92**, 064413 (2015).

[33] S. Okamoto, Spin injection and spin transport in paramagnetic insulators, Phys. Rev. B **93**, 064421 (2016).